Hindawi
Geofluids
Volume 2020, Article ID 8874403, 16 pages
https://doi.org/10.1155/2020/8874403

Research Article

Features and Constitutive Model of Gypsum's Uniaxial Creep Damage considering Acidization

Wei Chen,[1] **Wen Wan**,[1] **Senlin Xie**,[2] **Wenlong Kuang**,[1] **Wenqing Peng**,[1] **Qiuhong Wu**,[3] **Shasha Tong**,[4] **Xianqing Wang**,[1] **and Xiaoyu Tang**[1]

[1]*School of Resource, Environment and Safety Engineering, Hunan University of Science and Technology, Xiangtan, Hunan 411201, China*
[2]*School of Energy and Mining Engineering, China University of Mining and Technology (Beijing), Beijing 100083, China*
[3]*Work Safety Key Lab on Prevention and Control of Gas and Roof Disasters for Southern Coal Mines, Hunan University of Science and Technology, Xiangtan, Hunan 411201, China*
[4]*Foreign Language School, Hunan University of Science and Technology, Xiangtan, Hunan 411201, China*

Correspondence should be addressed to Wen Wan; wanwenhunst@163.com

Received 3 August 2020; Revised 21 August 2020; Accepted 27 August 2020; Published 22 September 2020

Academic Editor: Yixian Wang

Acidic fluids cause rock erosion and further endanger the safety of rock engineering, especially the corrosion of pillars by acidic or weakly acidic groundwater. In this paper, the rock samples in the gypsum mining area were taken as the research object. Uniaxial compression creep tests were carried out under neutral water, pH = 6 and pH = 5 hydrochloric acid solutions, respectively. Meanwhile, the specimens before and after saturation were observed by an electron microscope scanner. The results show that (1) the gypsum specimens with pH = 5 hydrochloric acid were damaged at the first stress level, while that with pH = 6 and pH = 7 were destroyed at the second stress level. The failure modes of the three groups were basically the same, with cleavage and end damage of different degrees. The difference is that the failure time of the former is earlier than that of the latter, which indicates that the stronger acidity causes greater corrosion on the creep of the samples. (2) From the perspective of microstructure, the samples saturated in the neutral aqueous solution and dry state are compact and complete in structure, and the whole is relatively homogeneous. However, after saturating in the acid solution, the samples significantly increased dense pores with large size and loose structure. Due to the rapid increase, the surfaces of the samples are almost like "holes". (3) A new nonlinear creep constitutive model was established by connecting Burgers model with nonlinear viscoplastic body (NVPB) model in series, which can well describe the creep characteristics of gypsum rocks under acid corrosion.

1. Introduction

Currently, about 44 percent of mines are exploited by the room-and-pillar method. French Lorraine iron ore accounts for 94% of the total production, while 58 mines in Lorraine are mined by the room-and-pillar method. In the United States, the method is used by 65 percent of metal mines and in Sweden, by over half of nonferrous metal mines [1, 2]. During the mining, accidents are not uncommon, which threaten the engineering quality and the safety of miners and even bring substantial economic losses to the country [3–6]. The potential safety hazard of the method is mainly manifested as: the pillar is eroded and becomes sharp (see Figure 1), which leads to the overall instability of the house [7–10].

With the massive mining, shallow mineral resources are gradually exhausted, pushing the mining to the deep, where the underground environment becomes increasingly complex [11–16]. After excavation, due to the existence of groundwater, the pillar will be eroded, leading to the gradual decrease of its stability with time and the eventual failure [17–19]. In the process of being eroded to destruction, the influence of groundwater and mine pressure on pillar cannot be ignored [3, 4, 20]. Especially, the groundwater with partial

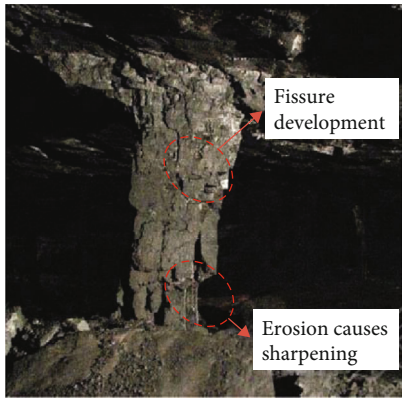

Figure 1: The mine pillar is eroded and sharpened.

acidity will seriously threaten the pillars [21–23]. Generally, the causes of the formation of groundwater are man-made and natural. Artificial acid groundwater is generally formed by the interaction of oxygen-containing water with surrounding rocks during mining [24, 25]. The naturally formed acidic groundwater is due to the long-term evolution of water environment under natural conditions [26–29] and causes damage to the mechanical properties of rocks, which is an inescapable problem [12, 30–33].

Wawersik et al. [34] conducted tests on granite and sandstone, and the results showed that the time-varying effect would enhance with moisture content. Under uniaxial compression, the steady-state creep rate of dry specimens differs by about two orders of magnitude from that of saturated specimens. The tests by Dong et al. [35] showed that the intrusion of groundwater into rocks mainly produces two effects: one is that the friction and cohesion between the rock mineral grains decreases; the other is that it changes the mineral composition and microstructure, resulting in pores, caves, and cracks, which eventually leads to the softening of the rock and greatly reduce its strength. Taking tuff as the research object, Zhu et al. [36] carried out creep tests under dry and saturated state, respectively, and discussed the regularity of rock creep under water-bearing state. The result showed that, compared with the creep deformation, the water content slightly affects the instantaneous elastic deformation modulus, but greatly affect the ultimate creep deformation. By comparing the dry and saturated samples, the difference of their creep deformations was found to be 5-6 times. Huang et al. [37] conducted uniaxial compression creep tests on mudstone under different water-bearing conditions and found that with the increase of water content, the elastic modulus and uniaxial compressive strength greatly reduced, and the creep deformation and steady-state creep rate significantly increased. Li et al. [38] carried out creep tests on granite in air-dried and saturated states. The results showed that the long-term strength of the saturated granites was lower than the dried ones, while the creep rate and deformation are roughly larger. Liu et al. [39] used soft conglomerate to carry out single and biaxial creep tests to analyze the deformation characteristics of dry and saturated specimens. The instantaneous deformation modulus of the saturated conglomerate was found to be much lower than that of the dry state. Okubo et al. [40] carried out uniaxial compressive creep tests on tuff and andesite in dry and saturated state and studied their creep characteristics. The creep strain of rock in saturated state was found to be larger than that in dry, while the strength of creep failure is smaller. Xie et al. [41] performed chemical corrosion on porous limestone, and then carried out triaxial creep tests. The results showed that chemical reagent corrosion can increase the creep deformation and the permeability. Li et al. [42] executed shear creep tests on weak structural planes of sandstone under different moisture content. The result showed that the effect of moisture content on the shear creep deformation of weak structural plane is very significant. With the increase of water content, its deformation amount increases gradually, and the creep strength decreases. Moreover, the time reaching to a stable creep state increases continuously. Based on the engineering background of Wuhan Yuejiang Tunnel, Li et al. [43] carried out dry and saturated shear creep tests, respectively, and found that water can accelerate the creep strain rate and reduce the strength value of creep failure. Therefore, in engineering practice, the effect of water on sandstone creep cannot be ignored. Wang et al. [44] carried out triaxial creep tests on silty mudstone with dry and saturated state, respectively, to analyze the influence of water on its creep deformation and long-term strength. The result showed that the instantaneous strain, creep strain, and total strain of silty mudstone in dry state are all smaller than those in saturated, and water can lead to a significant change in its creep mechanical properties. Brzesowsky et al. [45] investigated the creep effects of the hydrochemical environment and stress state coupling effect on sandstone under compression. Most scholars study the creep of rock in the hydrochemical environment by hydration treatment before testing. Few researches perform the two tests simultaneously.

Constitutive model is the key and difficult point of rock creep [46]. Many scholars have established creep constitutive models of rock materials from different ways and achieved fruitful results, including empirical model, component combination model, and nonlinear theoretical model [47–49].

Empirical models are the simplest, which refers to the establishment of stress-strain-time function relationships based on test data by using mathematical methods. They can be obtained from different rock materials with different experimental conditions. At present, common empirical model equations are power type, exponential type, logarithmic type, and the combination of the three. The theory mainly includes aging, flow, reinforcement theory, and elastic continuation [46, 50]. Xu et al. [51] took granite as the research object and carried out creep tests and obtained the empirical formula of the negative exponential type by summing up. Jiang et al. [52] executed uniaxial creep tests on sandstone. By using the creep test data and substituting power function, the power function type empirical model was obtained. Singh et al. [53] and Mesri et al. [54] summed up the power function constitutive relation between strain and time by the consolidation creep test of clay. Li et al. [55] performed uniaxial creep tests on marble and obtained the empirical formula of the creep by fitting the test curve. Lu et al. [56] carried out three-axis consolidation undrained

creep tests on subgrade soft soil, which showed that the hyperbolic empirical formula can well describe the relationship between time and strain. Zhang et al. [57] perform triaxial compression creep tests on the mudstone sampled on-site with a self-made rock creep testing machine and established the strength model of the mudstone. Although the empirical model can be well fitted to the creep test curve, it can only reflect the creep characteristics of a particular rock under a specific state or stress path. It describes the decay and steady creep stages, while cannot describe the accelerated creep, which made it difficult to reflect the creep mechanism and characteristics inside the rock, so empirical models are rarely used at present.

Component combination models idealize the rock medium into basic elements in series or parallel to reflect the properties in the process of creep, such as elasticity, viscosity, and plasticity [58]. The combination model is characterized by its simple concept, which can reflect the creep characteristics of various rocks by changing the size, quantity, and combination mode of various mechanical parameters of the basic elements. Therefore, it is widely used. Currently, common component models include the Maxwell model, Kelvin model, Bingham model, Burgers model, and Xiyuan model. Many studies on rock creep are based on element combination to describe the creep characteristics. Xia et al. [59] adopted the generalized Kelvin model and Xiyuan model to describe the creep characteristics of rocks in the Three Gorges lock regions. Peng et al. [60] conducted triaxial creep tests on mudstone and demonstrated the creep phenomenon with the Xiyuan model. Shen et al. [61] conducted a biaxial creep test on regular toothed structural planes and chose the Burgers model to reflect the creep characteristics of rock mass according to the test curve. Tao et al. [62] compared Burgers with Xiyuan, and the result showed that the Xiyuan model was more suitable for describing the creep characteristics of rock mass. However, these component models, composed of the linear combination of basic elements, can only reflect the decay and steady creep of the rock, but cannot reflect the accelerated creep.

The nonlinear creep model generally means that nonlinear elements are introduced to describe the accelerated creep characteristics of rock based on the linear combination model. Many scholars introduced nonlinear elements to properly combine linear and nonlinear elements, thus established a new creep model to better describe the three stages of rock creep. Chan et al. [63] and Boidy et al. [64] got the nonlinear creep equation through an in-depth study of the creep characteristics of nonlinear viscoelastic materials. Yuan et al. [65] proposed a plastic element based on the Mohr-Coulomb criterion and obtained an improved Burgers model, which can well describe the creep characteristics. Based on the creep test results of silty mudstone, Li et al. [66] introduced a nonlinear viscoplastic element in series to build a new nonlinear Burgers model to reflect the creep characteristics in the acceleration phase. Pan et al. [67] introduced nonlinear Bingham viscoplastic elements and Kelvin elements based on the Xiyuan model to build an unsteady Xiyuan viscoelastic plastic creep model that could fully reflect the whole process of creep. Yang et al. [68] proposed an element with an unsteady viscosity coefficient and introduced it into the Poting-Thomson model, thus establishing a model with fewer parameters that can well simulate the three creep stages. Yang et al. [69] deduced the nonlinear creep equation by analyzing the creep fracture process of fracture damage. Hu et al. [70] analyzed the creep test data of salt rocks under the joint action of temperature and triaxial pressure and introduced nonlinear elements into the Bingham model to accelerate the creeping stage, thus establishing the creep constitutive relation considering temperature damage. Zheng et al. [71] established a creep model with volume creep based on the Burgers model, to describe the creep behavior of cracked sandstone. Liu et al. [72] proposed a creep constitutive model that can analyze the creep of soft coal, including viscoelastic-plastic and damage characteristics. Wu et al. [73] combined fractional software element with hooker body, introduced relevant parameters and variables, and derived a new nonlinear creep constitutive equation with fractional derivative. Through validation with experimental data, this model can well describe the creep characteristics. Based on the fractional derivative creep model, Wang et al. [74] derived the nonlinear creep constitutive equation of coal under three-dimensional stress state. Yang et al. [75] introduced damage mechanics into the creep model and established a nonlinear damage creep model that can well describe decay, steady, and accelerated creep.

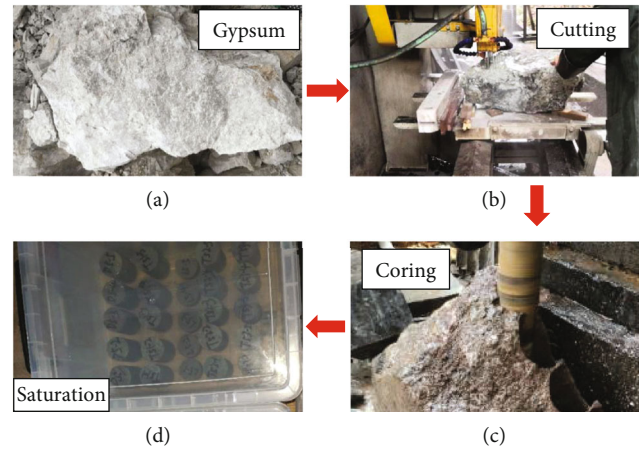

Figure 2: Gypsum specimens.

Great achievements have been made in creep tests and constitutive models of rocks under the influence of the hydrochemical environment [76]. However, most of the related studies are conducted on the acidification of rocks before the mechanical properties are tested, which is not quite consistent with the actual engineering [77]. The mine pressure and the immersion of groundwater continuously influence on the pillars. At present, the creep constitutive model of rock is mainly applied to the analysis of rock mass itself, but rarely to the external environmental factors such as acid, alkali, temperature, and humidity [78, 79]. Based on the abovementioned engineering

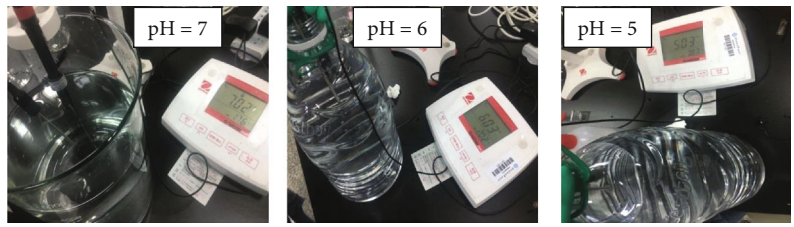

Figure 3: Preparation of hydrochloric acid solutions with different pH values.

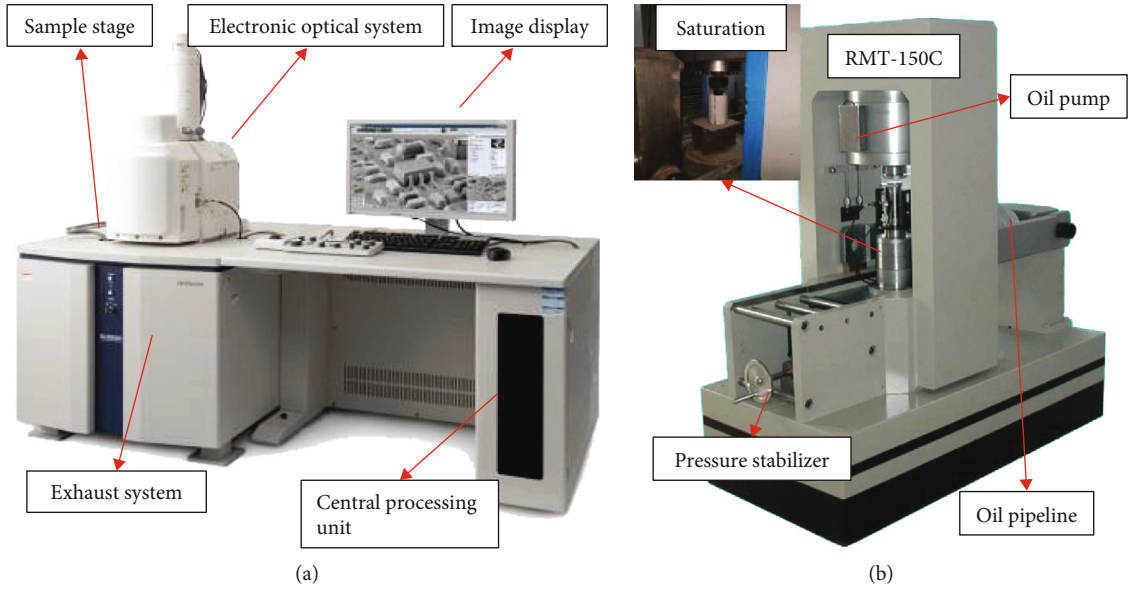

Figure 4: Equipment for tests. (a) SU3500: Hitachi gaoxin SEM. (b) RMT-150C: Rock mechanics test system.

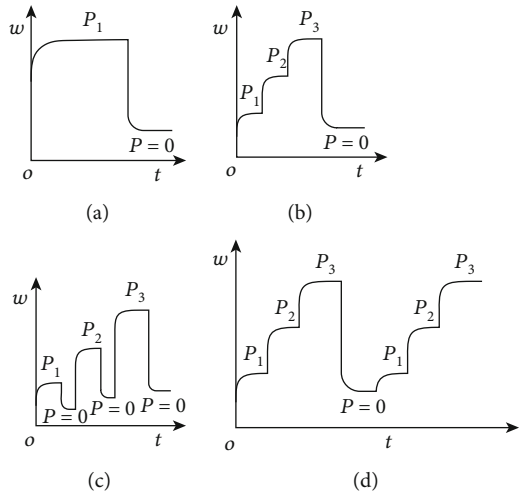

Figure 5: Loading methods for creep tests. (a) One-stage loading. (b) Multistage monotonic loading. (c) Multistage cyclic loading. (d) Specific loading methods of stress at various levels.

practice, the hydrogeological survey of the Gypsum mine in Lilin County, Hunan province, was carried out. Through investigation, weak acid groundwater was found in this mine area, where the pillar is damaged by its erosion for a long time. Therefore, this paper intends to take the gypsum rock in the mine area as the research object, simulate the groundwater erosion environment, conduct immersion on the gypsum rock, study the uniaxial compression creep mechanical characteristics and constitutive model of the gypsum rock under the condition of acid erosion, and thus provide certain guiding significance for the retaining and protection of pillars.

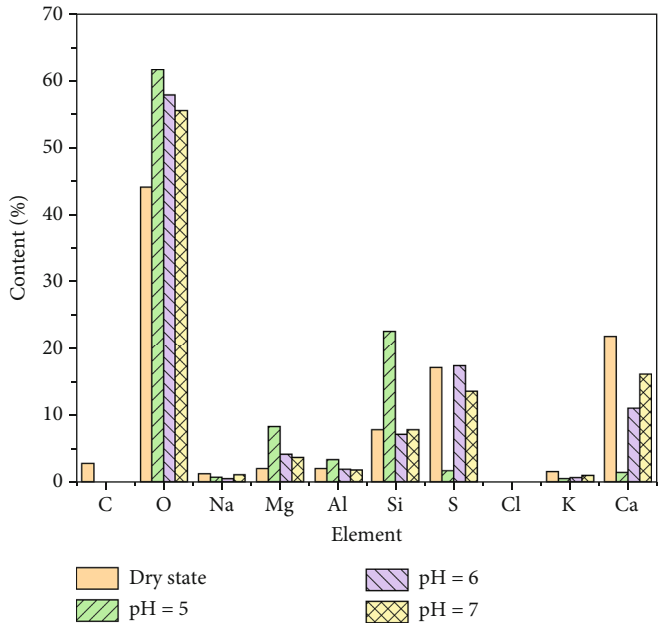

Figure 6: The content of elements on the rock surface under various experimental conditions.

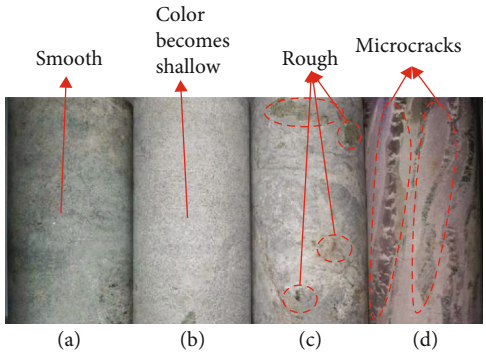

Figure 7: Macrocomparison of rock specimens before and after different saturations. (a) Naturally dry condition. (b) pH = 7. (c) pH = 6. (d) pH = 5.

2. Laboratory Tests

2.1. Preparation of Rock Specimens. All the specimens are taken from the gypsum mine in Lilin County, Changde, Hunan Province. To reduce the dispersion of rock specimens, we sample them from the same rock block by drilling and coring (see Figure 2(a)–2(c)). To be specific, we make their ends and sides flat with the cutting machine and grind them with sandpaper to ensure the integrity and smoothness. Finally, we obtain the 50 × 100 mm standard cylinder specimens with smooth surfaces. We prepare hydrochloric acid solutions with pH values of 5, 6, and 7 in advance, respectively (see Figure 3). Then, the processed specimens are put into the prepared acidic solutions (see Figure 2(d)).

2.2. Experiment Content and Test Method. To observe the mechanical properties of gypsum before and after the acidification treatment, the scanning electron microscope (SEM) observations (see Figure 4(a)) and uniaxial compression creep tests (see Figure 4(b)) are performed.

2.2.1. SEM Observation. To observe the changes in the gypsum rock microstructure before and after acid corrosion, we perform SEM tests on four kinds of specimens. One is the original gypsum specimen in dry state, and the others are the specimens after the saturation with pH values of 7, 6, and 5 for 49 days, respectively. The sample surfaces are scanned with a magnification coefficient of 400-450 (see Figure 4(a)).

2.2.2. Uniaxial Compression Creep Test. There are many loading methods for creep tests, among which one-stage loading, multistage monotonic loading, and multistage cyclic loading are commonly used [80] (see Figures 5(a)–5(c)).

The uniaxial compression creep tests are carried out on RMT-150C rock mechanics testing machine in the Hunan University of Science and Technology (see Figure 4(b)). Considering the dispersion of the samples and the addition of acid solutions, we combine the multistage monotonic loading (see Figure 5(b)) with the multistage cyclic loading (see Figure 5(c)) in this test and call them the multistage monotonic cyclic loading mode (see Figure 5(d)). The stress in uniaxial compression creep tests is divided into three levels: 50%, 60%, and 70% of the uniaxial compressive strength. Since the previously measured average uniaxial compressive strength of gypsum rock is 64 MPa, the three stress levels are set to 32 MPa, 38.4 MPa, and 44.8 MPa, respectively. Each stress level is maintained for 48 h. After the first monotonic loading stage, we unload the stress to 0.1 kN for 24 h and observe the unloading curve. Then, we add the hydrochloric acid solution with pH values of 5, 6, and 7 into the molds, which are divided into the first, the second, and the third group. Next, we carry out the second stage loading on the specimens and observe the change of the stress-strain curves. Note that the stress level and the holding time are the same as in the first stage.

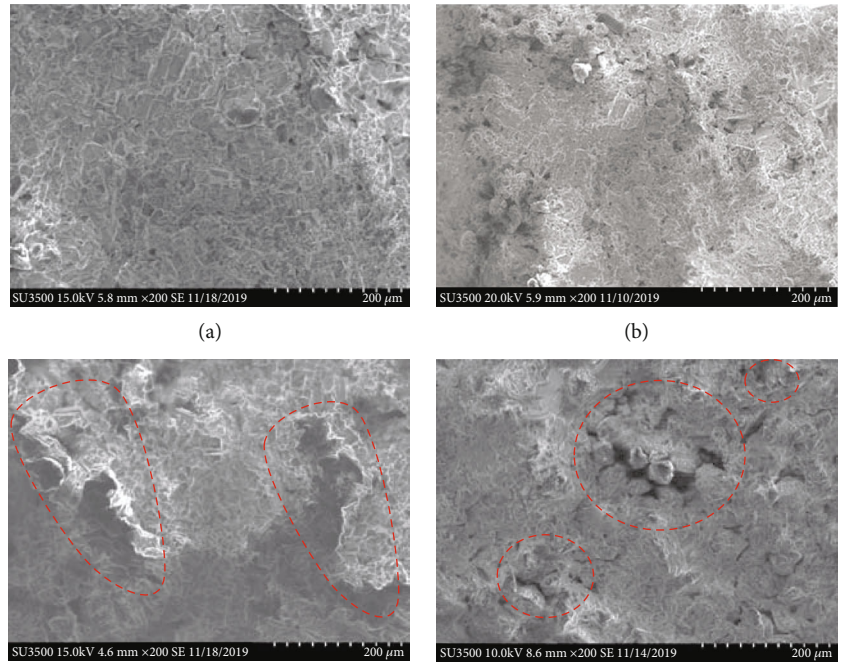

Figure 8: Enlarged microstructures of rock samples with different saturations. (a) Naturally dry condition. (b) pH = 7. (c) pH = 6. (d) pH = 5.

3. Laboratory Results and Discussion

3.1. Chemical Damage Analysis. The main component of gypsum is $CaSO_4$. However, there exist other oxides in gypsum rocks, such as SiO_2 and CaO. As the reaction goes on, the contents of Ca, K, and Na in the gypsum rock decrease, while the proportion of Si and Mg increases. It is because the reaction of hydrochloric acid with $CaSO_4$ and other substances forms solutions or gas. The nonhydrophilic minerals or the minerals that cannot react with hydrochloric acid will be exposed on the rock surface. Since the acidity affects the reaction efficiency, the proportions of elements are different under the four conditions (see Figure 6). In the acidic solutions, the oxidized mineral of gypsum reacts with H^+ as follows:

$$\begin{aligned} CaSO_4 + 2H^+ &== Ca^{2+} + H_2SO_4 \\ SiO_2 + 4H^+ &== Si^{4+} + 2H_2O \\ Al_2O_3 + 6H^+ &== 2Al^{3+} + 3H_2O \\ Na_2O + 2H^+ &== 2Na^+ + H_2O \\ CaO + 2H^+ &== Ca^{2+} + H_2O \\ K_2O + 2H^+ &== 2K^+ + H_2O \\ MgO + 2H^+ &== Mg^{2+} + H_2O \end{aligned} \quad (1)$$

3.1.1. Rock Surface Characteristics after Acidification. From the macroscopic point of view, the outer surface of gypsum rock is smooth after being cored, cut, and polished (see Figure 7(a)). After being saturated in the acid solution with pH = 5 or 6, the protective layer of the rock specimen falls off from the outer surface. The new surface becomes rough, and the size of the specimen becomes a little smaller (see Figures 7(c) and 7(d)). The rock specimen saturated in the distilled water (pH = 7) has no obvious change in size, but it changes in color (see Figure 7(b)). Compared with the specimen saturated in the acid solution with pH = 6 (see Figure 7(c)), the one in the solution with pH = 5 has more powdery particles falling off its surface and has fine cracks (see Figure 7(d)). Therefore, the acid solution with the lower pH value causes stronger chemical damage to the gypsum.

Microscopically, the rock specimen shows a clear layered structure and lamellar crystalline morphology before immersion. It has good homogeneity, close internal structure, and small interlayer distance. The microfracture and micropore are of small size and relatively scattered distribution. There is almost no large pore in the specimens (see Figure 8(a)). It means that the gypsum rocks have good macroscopic mechanical properties before erosion.

After being saturated in the neutral water, the structure of the specimen does not change significantly, but the color became lighter (see Figure 8(b)). After being saturated in the acid solution, the original lamellar structure or lamellar crystal morphology changes to sponge or floc shape, the structural porosity increases, and the interlayer boundary becomes fuzzy (see Figure 8(c)). The numbers of microcracks and micropores increase, and some independent small-sized micropores are connected to form large-scale "gullies" (see Figure 8(d)). Besides, the solution with the lower pH value causes more serious damage to the internal microstructure.

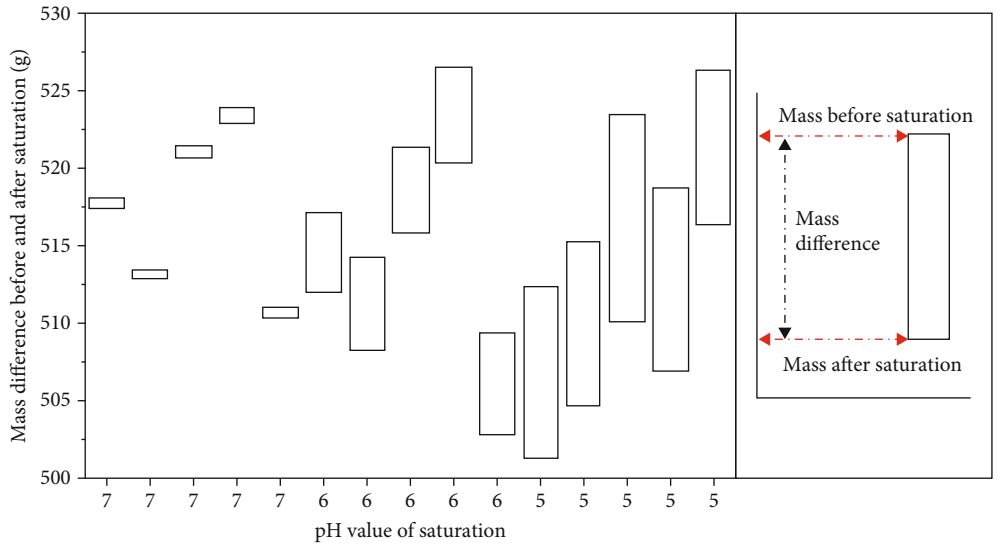

Figure 9: Comparisons of the mass changes with different saturations.

Table 1: Creep damage of gypsum rocks under different situations.

pH value	1st stress level (32 MPa)	2nd stress level (38.4 MPa)	3rd stress level(44.8 MPa)
7	No damage occurs	Damage occurs after loading for about 262.3 h	—
6	No damage occurs	Damage occurs after loading for about 242.7 h	—
5	Damage occurs after loading for about 180.6 h	—	—

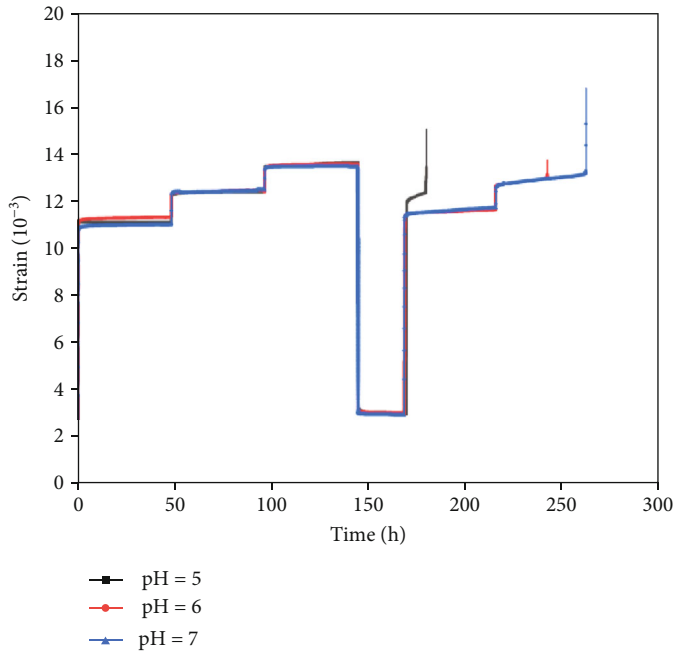

Figure 10: Comparison of uniaxial compression creep curves of gypsum under different situations.

From the microscopic point of view, it proves that the stronger acidity of the solution can aggravate the damage of the mechanical properties of gypsum.

3.1.2. Mass Damage after Acidification. Five samples were randomly selected from the three groups. Comparisons between the mass before and after saturation with different pH values are shown in Figure 9. The sample masses of the three groups decrease in various degrees. With the decrease of the pH value, the decline of the mass increases. It indicates that the higher concentration of H^+ in the solution causes a more intense and rapid reaction between the specimen and

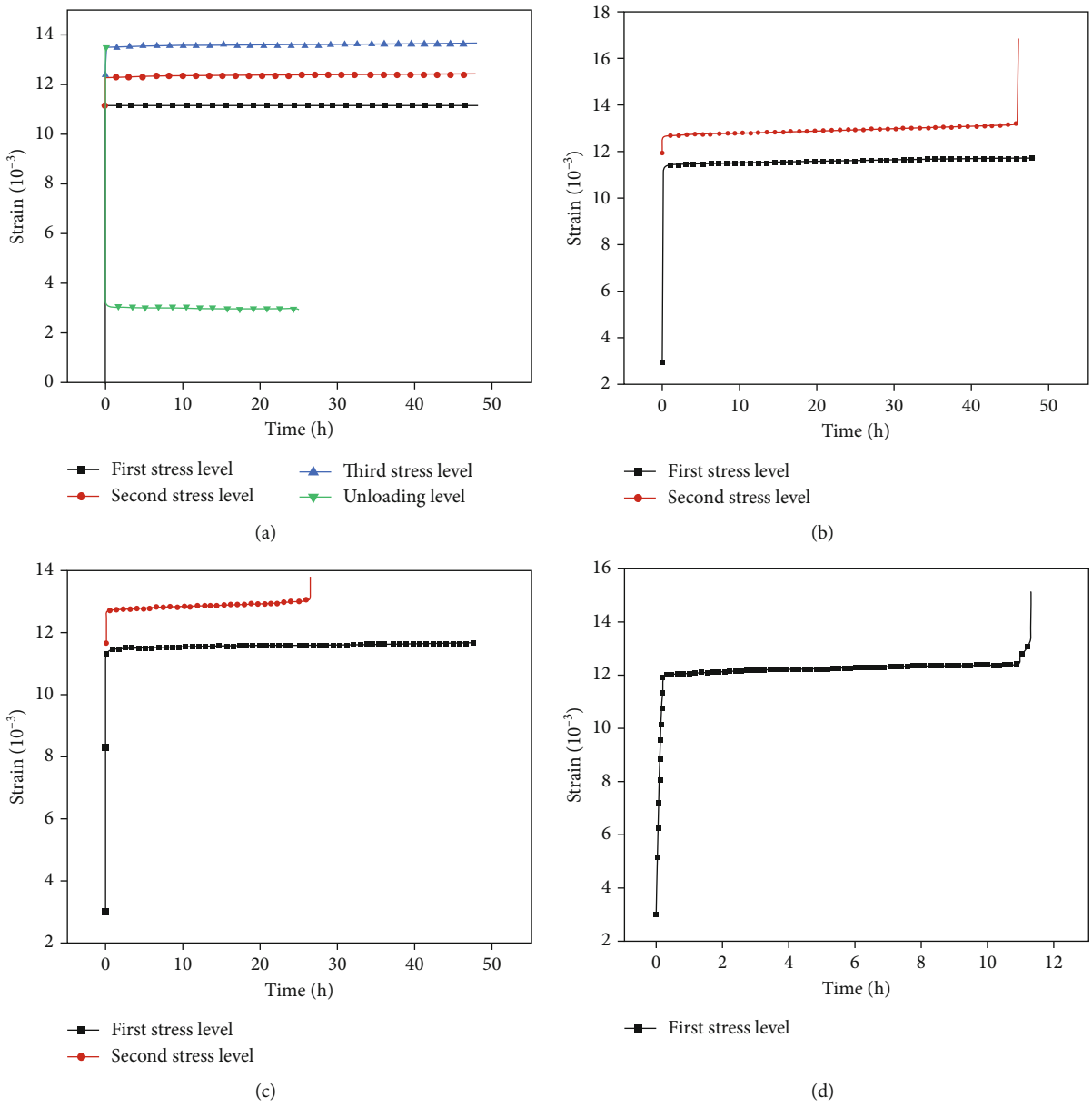

Figure 11: Creep curves at different stress levels of gypsum rock. (a) Samples in dry state during the whole loading processes. (b) Sample soaked with distilled water during the second loading process. (c) Sample under the pH = 6 acidic solution during the second loading process. (d) Sample under the pH = 5 acidic solution during the second loading process.

the solution [81]. This phenomenon also reflects that more serious damage will occur to the microstructure of gypsum with stronger acidity. Note that the quality of the specimens saturated in the distilled water also decreases slightly. Thus, there exist water-soluble minerals in the gypsum.

3.2. Analysis of Uniaxial Compression Creep Tests of Gypsum under Acid Corrosion

3.2.1. Uniaxial Creep Mechanics and Deformation Characteristics of Gypsum. Through three groups of uniaxial compression creep tests under acid corrosions, we obtain data of gypsum in terms of different pH values. Considering the discreteness of the samples, we choose the specimen with the ideal result from each test group and make analysis. Table 1 shows the creep damage of gypsum rocks, and Figure 10 illustrates the creep curve of the specimens under different acid conditions.

When the three groups of specimens loaded with three levels of stress in the first loading process, their strain increments have nearly no difference. When the axial stress is unloaded to the preload value, there exist residual deformations in the specimens, which are almost the same (see Figure 10). It means that the dispersion of the three groups is small, and the test results are reliable. During the second loading process, the specimen soaked in the solution with pH = 5 is damaged under the first stress level, whereas the specimen soaked in the solution with pH = 6 and the one

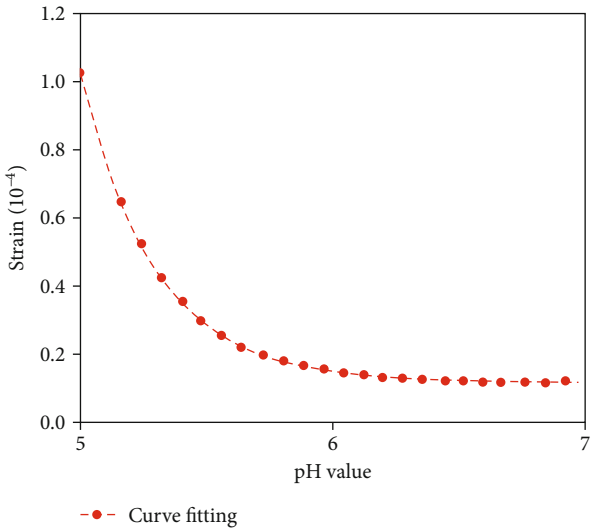

Figure 12: Strain rate during steady-state creep under different solutions.

soaked in distilled water both failed under the second stress level. The difference is that the former specimen is damaged earlier than the latter, which confirms that the stronger acidity causes greater creep damage. According to the test data, we draw the creep curves of specimens under different stress levels (see Figure 11) and analyze the test results in detail.

In the first loading process, the rocks have instantaneous strain when they are under axial stress. For the three groups of specimens in the dry state, when the stress is 32 MPa, their instantaneous axial strains are 1.10%, 1.00%, and 1.09%. As time goes on, the increase of the strains becomes more slowly, and the final strains are stable at 1.11%, 1.13%, and 1.10%, respectively. When the stress increases to 38.4 MPa, the instantaneous strain increments are 0.11%, 0.10%, and 0.13%, respectively. The strains increase more slowly with time, and the final strain increments are stable at 0.13%, 0.12%, and 0.15%, respectively. When the stress increases to 44.8 MPa, the instantaneous strain increments are 0.10%, 0.09%, and 0.09%, respectively. The strain increases slowly with time, and the final strain increments are stable at 0.13%, 0.11%, and 0.10%. With axial stress loading, the strains increase slowly with time, while the growth rate decreases. When the growth rate is zero, the specimen goes into a stable creep state. When the stress increases from the first level to the second level, the strain increment of specimens is greater, compared to the case that the stress increases from the second level to the third level. This indicates that the specimens are fully compacted under the second stress level instead of the first.

In the unloading process, the strains of the three groups of specimens all drop sharply to about 0.29% and then go into the stable stage. The deformations of the specimens are not fully recovered. Residual deformations still exist. It indicates that the specimens suffer plastic deformation (see Figure 11(a)).

In the second loading process, we add different solutions into the molds. The rock specimen soaked in the pH = 5 solution shows the most obvious change. After being loaded with the first stress level, the rock sample is damaged after 11.3 h. At the beginning of loading, the instantaneous strain appears and grows from 0.29% to 1.19%. It can be seen from Figure 11(d) that the first creep stage is very short. The specimen soon enters the steady-state creep stage, during which the strain rate is almost unchanged and keeps at about 1.03×10^{-4}/h. After about 11 h, the specimen goes into the accelerated creep stage. At this time, the strain begins to accelerate, the strain rate increases, the creep curve becomes concave, and the specimen is damaged quickly. As for the specimen soaked in the solution with pH = 6 and the one soaked in the neutral distilled water, their initial creep stages are very short under the first stress level. They enter the steady-state creep stage quickly and do not have the accelerated creep stage. Under the second stress level, these two groups of specimens experience the initial stage, steady stage, and accelerated creep stage. Their strain rates in the steady creep stage are 1.46×10^{-5}/h and 1.16×10^{-5}/h, respectively. Besides, the specimen saturated in the acid solution is destroyed much earlier than the one soaked in neutral distilled water (see Figures 11(b) and 11(c)).

We compare the strain rates of rock specimens in the steady-state creep stage before entering the accelerated creep stage. As shown in Figure 12, the saturation with the smaller pH value produces greater strain rate. With the decrease of the pH value, the strain rate increases exponentially. It shows that hydrochloric acid affects the creep characteristics of gypsum, which can accelerate the creep. To be specific, the stronger acidity causes greater influence on the creep damage.

3.2.2. Uniaxial Creep Failure Patterns of Gypsum under Acid Corrosion. In different external environments, the rocks present different failure patterns [82]. As for the three groups of gypsums under acid corrosion, their uniaxial creep failure patterns are roughly the same (see Figure 13). All of them suffer splitting failure modes and end damages with different degrees. Especially, the specimen saturated in the acid solution with pH = 5 is most clearly destroyed. Since some minerals in specimens can react with hydrochloric acid and change into solution and gas, the end of specimens becomes sharper after the reaction. Moreover, with the axial stress, the rock specimens are finally destroyed. It can be seen from the damage degrees that the solution with the smaller pH value has more obvious effect on the creep characteristics of gypsum.

3.3. The Creep Constitutive Model of Gypsum under Acid Corrosion. Under the external loads, rocks show complex mechanical characteristics, such as elasticity, plasticity, and creep. In the study of creep characteristics, the most important parts are the creep model construction and application [83]. To describe different creep characteristics of rocks, researchers usually take the methods of empirical formulas and differential equations. Based on the experimental data of the uniaxial compression creep of gypsum obtained in the previous sections, we introduce a nonlinear element and combine it with basic elements to establish a new constitutive model. The model can describe the accelerated creep stage of gypsum under the acid solution.

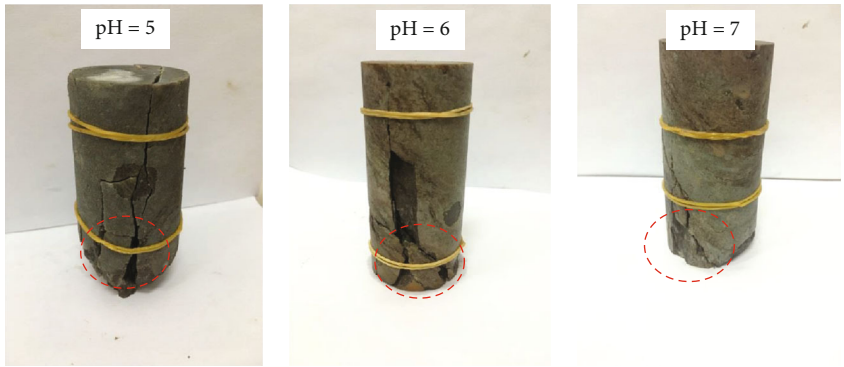

Figure 13: Uniaxial creep failure pattern of gypsum under acid corrosion. (a) Sample under the pH = 5 acidic solution. (b) Sample under the pH = 6 acidic solution. (c) Sample soaked with distilled water.

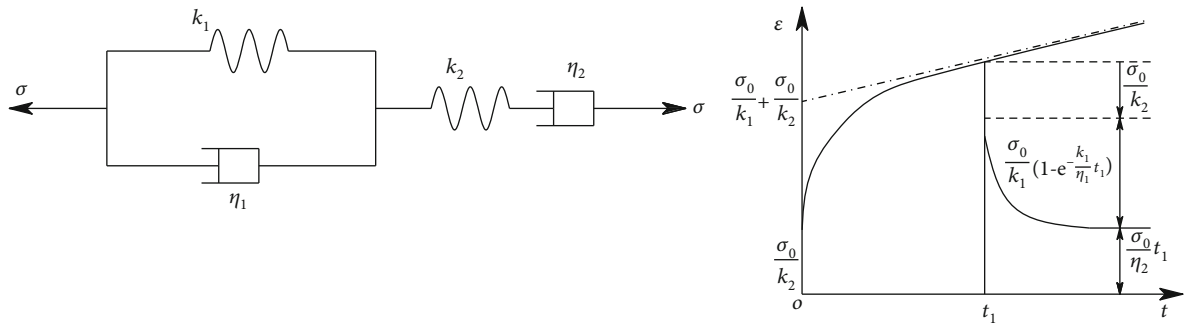

Figure 14: Burgers mechanic model and dynamics. (a) Burgers mechanics model. (b) Burgess creep and unload curve.

3.3.1. Establishment of the Uniaxial Compression Creep Model of Gypsum under Acid Corrosion. The Burgers model is a viscoelastic model composed of the Kelvin model and Maxwell model in series [84, 85]. Its mechanic model and dynamics are shown in Figure 14.

The constitutive equation of the Kelvin model is

$$\sigma_1 = \eta_1 \varepsilon_1{}' + k_1 \varepsilon_1. \tag{2}$$

The constitutive equation of the Maxwell model is

$$\varepsilon_2{}' = \frac{\sigma_2{}'}{k_2} + \frac{\sigma_2}{\eta_2}. \tag{3}$$

According to the series relation, there is

$$\varepsilon = \varepsilon_1 + \varepsilon_2, \varepsilon' = \varepsilon_1{}' + \varepsilon_2{}'; \sigma = \sigma_1 = \sigma_2 = \eta_1 \varepsilon_1{}' + k_1 \varepsilon_1. \tag{4}$$

According to equations (2), (3), and (4), we can get:

$$\sigma = \eta_1 \varepsilon' - \eta_1 \left(\frac{\sigma'}{k_2} + \frac{\sigma}{\eta_2} \right) + k_1 (\varepsilon - \varepsilon_2). \tag{5}$$

By differentiating and simplifying equation (5), we get the constitutive equation of the Burgers model as

$$\sigma'' + \left(\frac{k_2}{\eta_1} + \frac{k_2}{\eta_2} + \frac{k_1}{\eta_1} \right) \sigma' + \frac{k_1 k_2}{\eta_1 \eta_2} \sigma = k_2 \varepsilon'' + \frac{k_1 k_2}{\eta_1} \varepsilon'. \tag{6}$$

The creep equation of the Kevin model is

$$\varepsilon_1 = \frac{\sigma_0}{k_1} \left(1 - e^{-\frac{k_1}{\eta_1} t} \right). \tag{7}$$

The creep equation of the Maxwell model is

$$\varepsilon_2 = \frac{\sigma_0}{k_2} + \frac{\sigma_0}{\eta_2} t. \tag{8}$$

According to the superposition principle, the creep equation of the Burgers model can be obtained by superimposing the creep equations of the Kelvin and Maxwell models as

$$\varepsilon = \frac{\sigma_0}{k_2} + \frac{\sigma_0}{\eta_2} t + \frac{\sigma_0}{k_1} \left(1 - e^{-\frac{k_1}{\eta_1} t} \right). \tag{9}$$

According to equation (9), when $t = 0$, there is

$$\varepsilon_0 = \frac{\sigma_0}{k_2}. \tag{10}$$

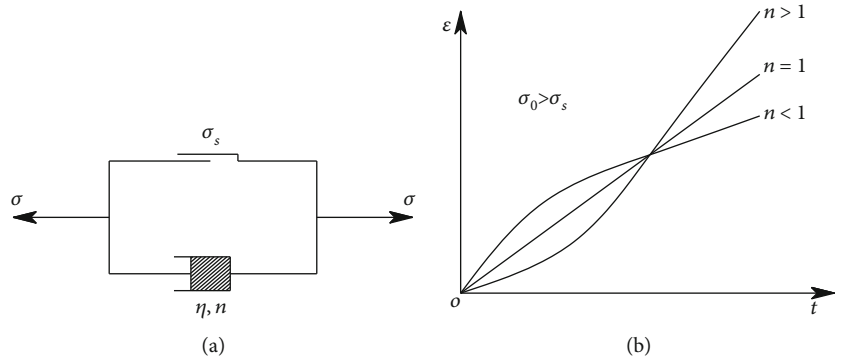

Figure 15: (a) Nonlinear viscoplastic body (NVPB). (b) Creep curve of the NVPB model.

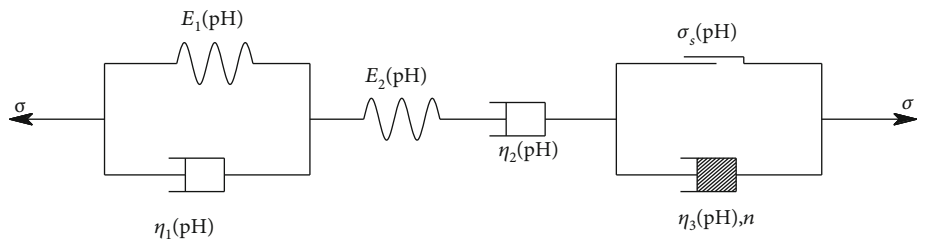

Figure 16: Nonlinear creep constitutive model of gypsum rock under acid corrosion.

It means that the burgers model has instantaneous elastic deformation. Besides, when $t = 0$, no other component except the spring k_2 has deformation. As time goes on, the strain increases, and the viscous element flows at a constant velocity.

At the moment of t_1, the unloading process begins. Its curve is shown in Figure 14(b). During the unloading process, the instantaneous spring back happens on the spring k_2. With the increase of time, the deformation of k_2 continues to recover until the deformation of spring k_2 restores. At this time, the deformation is

$$\varepsilon_0 = \frac{\sigma_0}{k_1}\left(1 - e^{-\frac{k_1}{\eta_1}t}\right). \tag{11}$$

When t_1 is large enough, the deformation recovery of the elastic after effect is

$$\varepsilon_0 = \frac{\sigma_0}{k_1}. \tag{12}$$

Finally, the remaining deformation of the model is

$$\varepsilon_0 = \frac{\sigma_0}{\eta_2}t_1. \tag{13}$$

The above analysis shows that this model has the characteristics of instantaneous deformation, deceleration creep, and constant velocity creep.

According to the above test results, under the condition of acid corrosion and low stress, the gypsum rocks have instantaneous deformation and suffer the deceleration and stable creep stages. Under the condition of high stress, the rocks also have instantaneous deformation and suffer the deceleration creep, stable creep, and accelerated creep stages. Although the Burgers model can well reflect the properties of instantaneous deformation, deceleration creep, and stable creep, it cannot represent the accelerated creep stage. Therefore, based on the Burgers model, this paper constructs a new model to describe the characteristics of gypsum rocks in different creep stages under acid corrosion.

Under the corrosion of acid, the mechanical properties of gypsum become weaker. At the same time, the external stress makes the internal structure of rock dislocated [86]. The creep failure of the specimen finally occurs under the combined action of force and acid. Since there exists acidification in the whole creep process, the parameters that reflect the creep characteristics of gypsum rocks must be related to the pH value. The main creep parameters related to the pH value are the elastic modulus and viscosity coefficient of the gypsum rock. In the accelerated creep stage, the presence of acid can promote the accelerated creep process and rock failure. Xu et al. [87] proposed a new nonlinear viscoplastic body (NVPB) model by paralleling a nonlinear viscous element with a plastic element. NVPB can well reflect the accelerated creep stage of rock. Its mechanical model and creep curve are shown in Figure 15. In this paper, we will use this model to describe the accelerated creep stage of gypsum rocks under acid corrosion.

The creep equation of the model is

$$\varepsilon(t) = \begin{cases} 0 & (\sigma_0 \le \sigma_s) \\ \dfrac{\sigma_0 - \sigma_s}{\eta}t^n & (\sigma_0 > \sigma_s) \end{cases}. \tag{14}$$

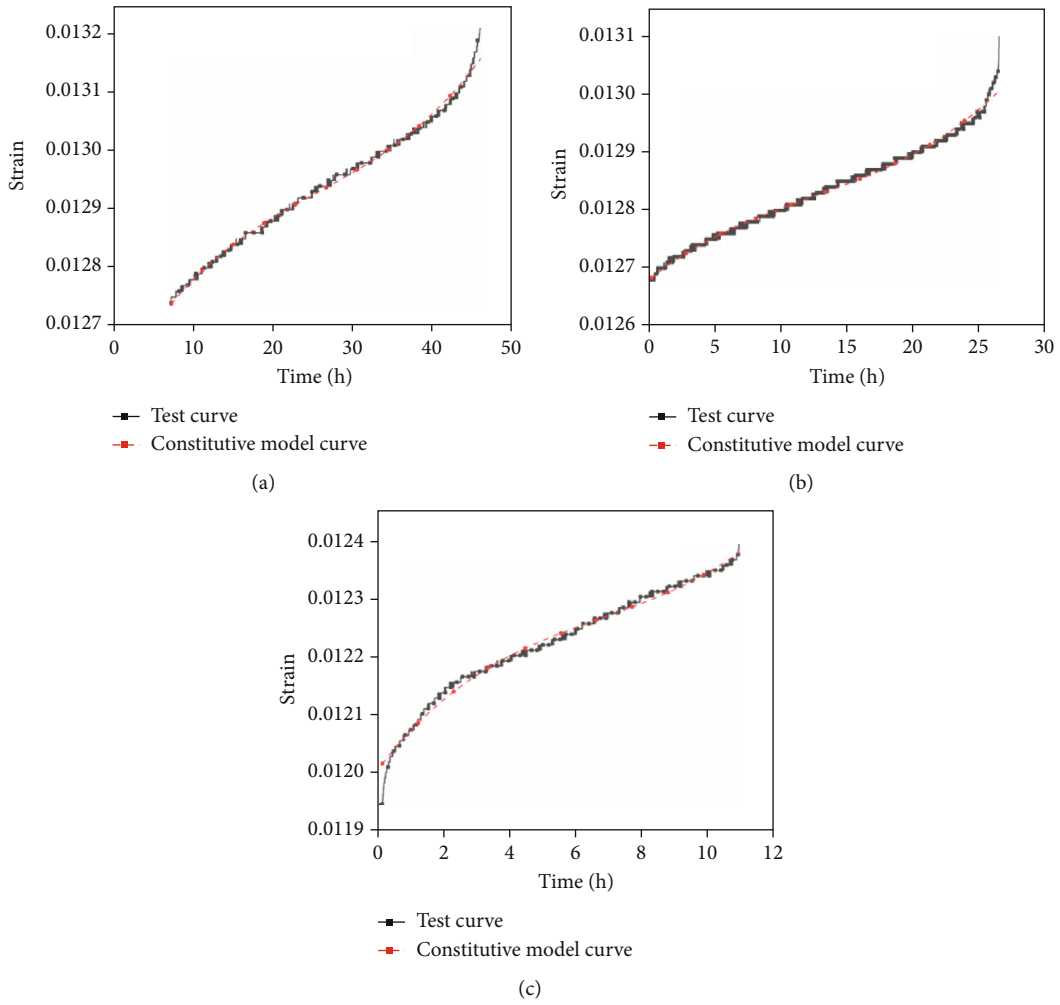

Figure 17: Creep test and constitutive model curves of samples under different pH conditions. (a) Sample soaked with distilled water. (b) Sample under the pH = 6 acidic solution. (c) Sample under the pH = 5 acidic solution.

When $n \neq 1$, the relationship between time and strain is nonlinear. When $n > 1$, the strain rate increases with time. When $n < 1$, the strain rate decreases with time. When the model is used to describe the accelerated creep stage of gypsum rock, n must be greater than "1". In this equation, η is the viscosity coefficient. Since this model is used to describe the creep characteristics of the gypsum rock under acid corrosion conditions, η must be related to the pH value and the stress σ. That is, $\eta = \eta$ (pH, σ). As we know, the Burgers model can well describe the creep mechanical properties of gypsum rocks. Therefore, by connecting the NVBP model with the Burgers model in series, we obtain a nonlinear creep model that can fully reflect the accelerated creep stage of gypsum rocks under acid corrosion. The elastic modulus and viscosity coefficient in the Burgers model are related to the pH value of the acid solution, so the specific structure of the nonlinear creep model is shown as Figure 16.

According to the creep equation (9) of the Burgers model, the creep equation (14) of the NVBP model, and the series property, we get the creep equation of the nonlinear creep model as follows:

In this equation, $E_1(\mathrm{pH})$ and $E_2(\mathrm{pH})$ are the elastic modulus of the viscoelastic body and the elastic element under acid corrosion, respectively. $\eta_1(\mathrm{pH})$, $\eta_2(\mathrm{pH})$, and $\eta_3(\mathrm{pH})$ are the viscosity coefficients of viscoelastic body, viscous

$$\varepsilon(t) = \begin{cases} \dfrac{\sigma}{E_2(\mathrm{pH})} + \dfrac{\sigma}{\eta_2(\mathrm{pH})}t + \dfrac{\sigma}{E_1(\mathrm{pH})}\left(1 - e^{-\frac{E_1(\mathrm{pH})}{\eta_1(\mathrm{pH})}t}\right), \sigma \leq \sigma_s(\mathrm{pH}) \\ \dfrac{\sigma}{E_2(\mathrm{pH})} + \dfrac{\sigma}{\eta_2(\mathrm{pH})}t + \dfrac{\sigma}{E_1(\mathrm{pH})}\left(1 - e^{-\frac{E_1(\mathrm{pH})}{\eta_1(\mathrm{pH})}t}\right) + \dfrac{\sigma - \sigma_s}{\eta_3(\mathrm{pH})}t^n, \sigma > \sigma_s(\mathrm{pH}) \end{cases}. \quad (15)$$

element, and the NVPB model under acid corrosion, respectively. $\sigma_s(\mathrm{pH})$ is the yield strength of the gypsum rock under acid corrosion.

According to equation (15), when $\sigma \le \sigma_s(\mathrm{pH})$, the model degenerates to the Burgers model. Then, it can describe the properties of the gypsum rock in terms of deceleration creep and stable creep. When $\sigma > \sigma_s(\mathrm{pH})$, the model is a nonlinear creep model that can describe the accelerated creep stage.

3.3.2. Verification of the Creep Constitutive Model. By substituting the identified parameters into the above model, we can get the constitutive model curves. Figure 17 shows its comparisons with the test curves.

According to Figure 17, the established constitutive model curve and creep test curve have good coincidence under various conditions. It means that the creep process of gypsum rock under acid corrosion can be well described by connecting the Burgers model with the NVPB model proposed by Xu et al. [79]. Besides, the square of the parameter identification correlation coefficient approaches to "1", which also verifies the correctness and rationality of the new model.

4. Conclusions

In light of the above work, the main conclusions of this paper are as follows:

(1) After acidic saturation, the original lamellar structures and crystal forms were spongy or flocculent. The sample structure loosened, and the boundary between layers became fuzzy. Meanwhile, the number of microcracks and micropores increased, which weakened the macromechanical properties of the gypsum

(2) The gypsum specimens with pH = 5 hydrochloric acid were damaged at the first stress level, while that with pH = 6 and pH = 7 were destroyed at the second stress level. The difference is that the failure time of the former is earlier than that of the latter, which indicates that the stronger acidity causes greater corrosion on the creep of the samples

(3) The failure modes of the three groups were basically the same, with cleavage and end damage of different degrees. The damage to the end of gypsum sample with pH = 5 hydrochloric acid is the most obvious

(4) A new nonlinear creep constitutive model was established by using the Burgers model and NVPB model in series, which agrees well with the creep test results and provides guidance for practical calculation

Data Availability

The numerical data used to support the findings of this study have not been made available because the nature of this research and participants of this study did not agree for their data to be shared publicly.

Conflicts of Interest

The authors wish to confirm that there are no known conflicts of interest associated with this publication, and there has been no significant financial support for this work that could have influenced its outcome.

Acknowledgments

We thank Zhenming Dong and Jie Liu for the useful discussions and early contributions to the project and Min Wang for the very helpful comments on the manuscript as well as the referees for the very helpful and inspiring comments. This research was funded by the National Natural Science Foundation of China (Grants nos. 51774132, 51774131, 51904101, and 51974118) and the Natural Science Foundation of Hunan Province (Grants no. 2020JJ5188).

References

[1] H. Harraz, *Underground Mining Methods: Room and Pillar Method*, 2014.

[2] A. G. Protosenya and A. Shokov, "3D modeling of pillar parameters in ore mining with room-and-pillar method," *Gornyi Zhurnal*, vol. 2015, pp. 20–23, 2015.

[3] Y. Wang, H. Lin, Y. Zhao, X. Li, P. Guo, and Y. Liu, "Analysis of fracturing characteristics of unconfined rock plate under edge-on impact loading," *European Journal of Environmental and Civil Engineering*, vol. 23, pp. 1–16, 2019.

[4] H. Lin, H. Yang, Y. Wang, Y. Zhao, and R. Cao, "Determination of the stress field and crack initiation angle of an open flaw tip under uniaxial compression," *Theoretical and Applied Fracture Mechanics*, vol. 104, article 102358, 2019.

[5] R. Cao, P. Cao, H. Lin, G. W. Ma, X. Fan, and X. G. Xiong, "Mechanical behavior of an opening in a jointed rock-like specimen under uniaxial loading: experimental studies and particle mechanics approach," *Archives of Civil and Mechanical Engineering*, vol. 18, no. 1, pp. 198–214, 2018.

[6] Y. Zhao, L. Zhang, W. Wang, C. Pu, W. Wan, and J. Tang, "Cracking and stress–strain behavior of rock-like material containing two flaws under uniaxial compression," *Rock Mechanics & Rock Engineering*, vol. 49, no. 7, pp. 2665–2687, 2016.

[7] P. Waclawik, R. Snuparek, and R. Kukutsch, "Rock bolting at the room and pillar method at great depths," *Procedia Engineering*, vol. 191, pp. 575–582, 2017.

[8] X. Zhou, Y. Zhang, Q. Ha, and K. Zhu, "Micromechanical modelling of the complete stress–strain relationship for crack weakened rock subjected to compressive loading," *Rock Mechanics and Rock Engineering*, vol. 41, no. 5, pp. 747–769, 2008.

[9] C. Zhang, P. Zou, Y. Wang, T. Jiang, H. Lin, and P. Cao, "An elasto-visco-plastic model based on stress functions for deformation and damage of water-saturated rocks during the freeze-thaw process," *Construction and Building Materials*, vol. 250, article 118862, 2020.

[10] B. Yuan, L. Xiong, L. Zhai et al., "Transparent synthetic soil and its application in modeling of soil-structure interaction using optical system," *Frontiers in Earth Science*, vol. 7, p. 276, 2019.

[11] Y. Zhao, L. Zhang, J. Liao, W. Wang, Q. Liu, and L. Tang, "Experimental study of fracture toughness and subcritical crack growth of three rocks under different environments," *International Journal of Geomechanics*, vol. 20, no. 8, article 04020128, 2020.

[12] Y. Zhao, L. Zhang, W. Wang, Q. Liu, L. Tang, and G. Cheng, "Experimental study on shear behavior and a revised shear strength model for infilled rock joints," *International Journal of Geomechanics*, vol. 20, no. 9, article 04020141, 2020.

[13] W. Chen, W. Wan, Y. Zhao, and W. Peng, "Experimental study of the crack predominance of rock-like material containing parallel double fissures under uniaxial compression," *Sustainability*, vol. 12, no. 12, article 5188, 2020.

[14] X. Zhou, J. Zhang, L. Yang, and Y. Cui, "Internal morphology of cracking of two 3-d pre-existing cross-embedded flaws under uniaxial compression," *Geotechnical Testing Journal*, vol. 41, no. 2, article 20170189, 2018.

[15] X. Zhou, "Localization of deformation and stress–strain relation for mesoscopic heterogeneous brittle rock materials under unloading," *Theoretical and Applied Fracture Mechanics*, vol. 44, no. 1, pp. 27–43, 2005.

[16] Y. Zhao, Y. Wang, W. Wang, W. Wan, and J. Tang, "Modeling of non-linear rheological behavior of hard rock using triaxial rheological experiment," *International Journal of Rock Mechanics and Mining Sciences*, vol. 93, pp. 66–75, 2017.

[17] X. Zhou, L. Li, and F. Berto, "Cracking behaviors of rock-like specimens containing two sets of preexisting cross flaws under uniaxial compression," *Journal of Testing and Evaluation*, vol. 47, no. 2, pp. 20170358–20170867, 2019.

[18] H. Lin, W. Xiong, and Q. Yan, "Modified formula for the tensile strength as obtained by the flattened brazilian disk test," *Rock Mechanics and Rock Engineering*, vol. 49, no. 4, pp. 1579–1586, 2016.

[19] X. Zhou and H. Yang, "Dynamic damage localization in crack-weakened rock mass: strain energy density factor approach," *Theoretical and Applied Fracture Mechanics*, vol. 97, pp. 289–302, 2018.

[20] Y. Wang, H. Zhang, H. Lin, Y. Zhao, and Y. Liu, "Fracture behaviour of central-flawed rock plate under uniaxial compression," *Theoretical and Applied Fracture Mechanics*, vol. 106, article 102503, 2020.

[21] R. Cao, P. Cao, X. Fan, X. Xiong, and H. Lin, "An experimental and numerical study on mechanical behavior of ubiquitous-joint brittle rock-like specimens under uniaxial compression," *Rock Mechanics and Rock Engineering*, vol. 49, no. 11, pp. 4319–4338, 2016.

[22] Q. Wu, L. Chen, B. Shen, B. Dlamini, S. Li, and Y. Zhu, "Experimental investigation on rockbolt performance under the tension load," *Rock Mechanics and Rock Engineering*, vol. 52, no. 11, pp. 4605–4618, 2019.

[23] L. Dong, D. Sun, W. Shu, and X. Li, "Exploration: safe and clean mining on earth and asteroids," *Journal of Cleaner Production*, vol. 257, article 120899, 2020.

[24] Z. He, D. Xiang, Y. Liu, Q. Gao, and H. Bian, "Deformation behavior of coarse-grained soil as an embankment filler under cyclic loading," *Advances in Civil Engineering*, vol. 2020, Article ID 4629105, 13 pages, 2020.

[25] Y. Wang, H. Zhang, H. Lin, Y. Zhao, X. Li, and Y. Liu, "Mechanical behavior and failure analysis of fracture-filled gneissic granite," *Theoretical and Applied Fracture Mechanics*, vol. 108, article 102674, 2020.

[26] X. Zhou, G. Li, and H. Ma, "Real-time experiment investigations on the coupled thermomechanical and cracking behaviors in granite containing three pre-existing fissures," *Engineering Fracture Mechanics*, vol. 224, article 106797, 2020.

[27] Y. Zhao, L. Zhang, W. Wang, W. Wan, and W. H. Ma, "Separation of elastoviscoplastic strains of rock and a nonlinear creep model," *International Journal of Geomechanics*, vol. 18, no. 1, article 04017129, 2018.

[28] S. Yang, Y. Huang, and P. Ranjith, "Failure mechanical and acoustic behavior of brine saturated-sandstone containing two pre-existing flaws under different confining pressures," *Engineering Fracture Mechanics*, vol. 193, pp. 108–121, 2018.

[29] X. Zhou and H. Yang, "Micromechanical modeling of dynamic compressive responses of mesoscopic heterogenous brittle rock," *Theoretical and Applied Fracture Mechanics*, vol. 48, no. 1, pp. 1–20, 2007.

[30] Y. Zhao, L. Zhang, W. Wang, J. Tang, H. Lin, and W. Wan, "Transient pulse test and morphological analysis of single rock fractures," *International Journal of Rock Mechanics and Mining Sciences*, vol. 91, pp. 139–154, 2017.

[31] Q. Wu, X. Li, L. Weng, Q. Li, Y. Zhu, and R. Luo, "Experimental investigation of the dynamic response of prestressed rockbolt by using an SHPB-based rockbolt test system," *Tunnelling and Underground Space Technology*, vol. 93, article 103088, 2019.

[32] X. Zhou, "Dynamic damage constitutive relation of mesoscopic heterogenous brittle rock under rotation of principal stress axes," *Theoretical and Applied Fracture Mechanics*, vol. 54, no. 2, pp. 110–116, 2010.

[33] B. Yuan, M. Sun, Y. Wang, L. Zhai, Q. Luo, and X. Zhang, "Full 3D displacement measuring system for 3D displacement field of soil around a laterally loaded pile in transparent soil," *International Journal of Geomechanics*, vol. 19, no. 5, article 04019028, 2019.

[34] W. R. Wawersik, "Technique and apparatus for strain measurements on rock in constant confining pressure experiments," *Rock Mechanics*, vol. 7, no. 4, pp. 231–241, 1975.

[35] L. Dong, X. Tong, X. Li, J. Zhou, S. Wang, and B. Liu, "Some developments and new insights of environmental problems and deep mining strategy for cleaner production in mines," *Journal of Cleaner Production*, vol. 210, pp. 1562–1578, 2019.

[36] H. Zhu and B. Ye, "Experimental study on mechanical properties of rock creep in saturation," *Chinese Journal of Rock Mechanics and Engineering*, vol. 21, no. 12, pp. 1791–1796, 2002.

[37] X. Huang, C. Yang, J. Liu, X. He, J. Chen, and X. Duan, "Experimental study on mudstone's creep behavior under different water contents and its effect on casing damage," *Chinese Journal of Rock Mechanics and Engineering*, vol. 27, pp. 3477–3482, 2008.

[38] L. You, W. Zhu, S. Bai, and C. Yang, "Uniaxial experimental study on rheological properties of granite in air-dried and saturated states," *Chinese Journal of Rock Mechanics and Engineering*, vol. 22, no. 10, pp. 1673–1677, 2003.

[39] G. Liu, Y. Hu, F. Chen, and Z. Xu, "Rheological property of soft rock under multiaxial compression and its effect on design of arch dam," *Chinese Journal of Rock Mechanics and Engineering*, vol. 23, no. 8, pp. 1237–1241, 2004.

[40] S. Okubo, K. Fukui, and K. Hashiba, "Long-term creep of water-saturated tuff under uniaxial compression," *International Journal of Rock Mechanics and Mining Sciences*, vol. 47, no. 5, pp. 839–844, 2010.

[41] S. Xie, J. Shao, and W. Xu, "Influences of chemical degradation on mechanical behaviour of a limestone," *International Journal of Rock Mechanics and Mining Sciences*, vol. 48, no. 5, pp. 741–747, 2011.

[42] P. Li, J. Liu, J. Zhu, and H. J. He, "Research on effects of water content on shear creep behavior of weak structural plane of sandstone," *Rock & Soil Mechanics*, vol. 29, no. 7, pp. 1865–1871, 2008.

[43] N. Li, H. Xu, and B. Hu, "Shear creep characteristics of sandstone under dry and saturated states," *Rock & Soil Mechanics*, vol. 33, no. 2, pp. 439–443, 2012.

[44] Q. Wang, X. Hu, C. Xu, C. Zhou, C. He, and C. Ying, "Time-dependent behavior of saturated silty mudstone under different confining pressures," *Bulletin of Engineering Geology and the Environment*, vol. 79, no. 5, pp. 2621–2634, 2020.

[45] R. H. Brzesowsky, S. J. T. Hangx, N. Brantut, and C. J. Spiers, "Compaction creep of sands due to time-dependent grain failure: effects of chemical environment, applied stress, and grain size," *Journal of Geophysical Research: Solid Earth*, vol. 119, no. 10, pp. 7521–7541, 2014.

[46] C. Zhang, H. Lin, C. Qiu, T. Jiang, and J. Zhang, "The effect of cross-section shape on deformation, damage and failure of rock-like materials under uniaxial compression from both a macro and micro viewpoint," *International Journal of Damage Mechanics*, vol. 29, no. 7, pp. 1076–1099, 2020.

[47] C. J. Jia, W. Y. Xu, R. B. Wang, S. S. Wang, and Z. N. Lin, "Experimental investigation on shear creep properties of undisturbed rock discontinuity in baihetan hydropower station," *International Journal of Rock Mechanics and Mining Sciences*, vol. 104, pp. 27–33, 2018.

[48] H. Li and H. Li, "Mechanical properties and acoustic emission characteristics of thick hard roof sandstone in Shendong coal field," *International Journal of Coal Science & Technology*, vol. 4, no. 2, pp. 147–158, 2017.

[49] M. Trzeciak, H. Sone, and M. Dabrowski, "Long-term creep tests and viscoelastic constitutive modeling of lower paleozoic shales from the baltic basin, N poland," *International Journal of Rock Mechanics and Mining Sciences*, vol. 112, pp. 139–157, 2018.

[50] H. Zhou, C. P. Wang, B. B. Han, and Z. Q. Duan, "A creep constitutive model for salt rock based on fractional derivatives," *International Journal of Rock Mechanics and Mining Sciences*, vol. 48, no. 1, pp. 116–121, 2011.

[51] X. Ping and X. Xia, "Study on creep characteristics of granite in lock zone of three gorges project," *Journal of Yangtze Riverentific Research Institute*, vol. 12, no. 2, pp. 23–29, 1995.

[52] Y. Jiang, X. Xian, D. Xiong, and F. Zhou, "Study on creep behaviour of sandstone and its mechanical models," *Chinese Jounal of Geotechnical Engineering*, vol. 27, no. 12, pp. 1478–1481, 2005.

[53] A. Singh and J. K. Mitchell, "General stress-strain-time function for soils," *Journal of the Soil Mechanics and Foundations Division*, vol. 94, no. 1, pp. 21–46, 1968.

[54] G. Mesri, E. Febrescordero, D. R. Shields, and A. Castro, "Shear stress-strain-time behaviour of clays," *Géotechnique*, vol. 32, no. 4, pp. 407–411, 1981.

[55] H. Li, Z. Li, and C. Su, "Testing study on creep characteristics of marble," *Chinese Journal of Rock Mechanics and Engineering*, vol. 23, no. 22, pp. 3745–3749, 2004.

[56] P. Lu, J. Zeng, and Q. Sheng, "Creep tests on soft clay and its empirical models," *Rock & Soil Mechanics*, vol. 29, no. 4, pp. 1041–1052, 2008.

[57] X. Zhang, Y. Li, S. Zhang, and B. Huo, "Creep theory of soft rock and its engineering application," *Chinese Journal of Rock Mechanics and Engineering*, vol. 23, pp. 1635–1639, 2004.

[58] C. Wang, Y. Zhao, Y. Zhao, and W. Wan, "Study on the interaction of collinear cracks and wing cracks and cracking behavior of rock under uniaxial compression," *Advances in Civil Engineering*, vol. 2018, Article ID 5459307, 10 pages, 2018.

[59] X. Xia, P. Xu, and X. Ding, "Rheological characteristics of rock and stability rheological analysis for high slope," *Chinese Journal of Rock Mechanics and Engineering*, vol. 15, no. 4, pp. 312–322, 1996.

[60] S. Peng, X. Wang, X. Liu, and S. Zhao, "Research on rhelogical characteristics of rock in the weak coal-bearing strata," *Journal of China Coal Society*, vol. 21, no. 5, pp. 361–364, 2001.

[61] M. Shen and G. Zhu, "Testing study on creep characteristic of regularly dentate discontinuity," *Chinese Journal of Rock Mechanics and Engineering*, vol. 23, no. 2, pp. 223–226, 2004.

[62] B. Tao, F. Wu, G. Guo, and R. Zhou, "Flexibility of visco-elastoplastic model to rheological characteristics of rock and solution of rheological parameter," *Chinese Journal of Rock Mechanics and Engineering*, vol. 24, no. 17, pp. 3165–3171, 2005.

[63] K. S. Chan, S. R. Bodner, A. F. Fossum, and D. E. Munson, "A constitutive model for inelastic flow and damage evolution in solids under triaxial compression," *Mechanics of Materials*, vol. 14, no. 1, pp. 1–14, 1992.

[64] E. Boidy, A. Bouvard, and F. Pellet, "Back analysis of time-dependent behaviour of a test gallery in claystone," *Tunnelling and Underground Space Technology*, vol. 17, no. 4, pp. 415–424, 2002.

[65] H. Yuan, P. Cao, W. Xu, and Y. Chen, "Visco-elastop-lastic constitutive relationship of rock and modified burgers creep model," *Chinese Journal of Geotechnical Engineering*, vol. 28, no. 6, pp. 796–799, 2006.

[66] Y. Li, H. Yu, and H. Liu, "Study of creep constitutive model of silty mudstone under triaxial compression," *Yantu Lixue/Rock & Soil Mechanics*, vol. 33, no. 7, pp. 2035–2047, 2012.

[67] X. Pan, Z. Yang, and J. Xu, "Application study of nonstationary nishihara viscoelasto-plastic rheological model," *Chinese Journal of Rock Mechanics and Engineering*, vol. 30, pp. 2640–2646, 2011.

[68] G. Yang, W. Wang, D. Xiong, and X. Feng, "Study on nonlinear viscoelasto-plastic creep model of rock," *Journal of Hebei University of Engineering*, vol. 34, no. 4, pp. 23–26, 2017.

[69] Y. Yang, "The underlying relationship between nonlinear rheological property of fissured rocks and damage development," *Engineering Mechanics*, vol. 11, no. 2, pp. 81–90, 1994.

[70] Q. Hu, X. Feng, and H. Zhou, "Study of creep model of rock salt with thermal damage considered," *Yantu Lixue/Rock & Soil Mechanics*, vol. 30, no. 8, pp. 2245–2248, 2009.

[71] H. Zheng, X. T. Feng, and X. J. Hao, "A creep model for weakly consolidated porous sandstone including volumetric creep," *International Journal of Rock Mechanics and Mining Sciences*, vol. 78, pp. 99–107, 2015.

[72] C. Liu, F. Zhou, J. Kang, and T. Xia, "Application of a nonlinear viscoelastic-plastic rheological model of soft coal on borehole stability," *Journal of Natural Gas Science and Engineering*, vol. 36, pp. 1303–1311, 2016.

[73] F. Wu, J. Chen, and Q. Zou, "A nonlinear creep damage model for salt rock," *International Journal of Damage Mechanics*, vol. 28, no. 5, pp. 758–771, 2018.

[74] L. Wang, H. Zhou, T. Rong, and W. Ren, "Research on experimental and nonlinear creep constitutive model of coal at depth," *Journal of China Coal Society*, vol. 43, no. 8, pp. 2196–2202, 2018.

[75] S. Yang and P. Xu, "A new nonlinear rheological damage model for rock," *Chinese Journal of Geotechnical Engineering*, vol. 36, no. 10, pp. 1846–1854, 2014.

[76] S. Xie, H. Lin, Y. Chen, R. Yong, W. Xiong, and S. du, "A damage constitutive model for shear behavior of joints based on determination of the yield point," *International Journal of Rock Mechanics and Mining Sciences*, vol. 128, article 104269, 2020.

[77] Q. Wu, L. Weng, Y. Zhao, B. Guo, and T. Luo, "On the tensile mechanical characteristics of fine-grained granite after heating/cooling treatments with different cooling rates," *Engineering Geology*, vol. 253, pp. 94–110, 2019.

[78] H. Lin, W. Xiong, Z. Xiong, and F. Gong, "Three-dimensional effects in a flattened Brazilian disk test," *International Journal of Rock Mechanics and Mining Sciences*, vol. 74, pp. 10–14, 2015.

[79] R. Cao, P. Cao, H. Lin, C. Z. Pu, and K. Ou, "Mechanical behavior of brittle rock-like specimens with pre-existing fissures under uniaxial loading: experimental studies and particle mechanics approach," *Rock Mechanics and Rock Engineering*, vol. 49, no. 3, pp. 763–783, 2016.

[80] H. P. Chin and J. D. Rogers, "Creep parameters of rocks on an engineering scale," *Rock Mechanics and Rock Engineering*, vol. 20, no. 2, pp. 137–146, 1987.

[81] J. Liu, P. Li, L. Qiao, and J. Zhu, "Experimental research on creep behavior and mechanism of sandstones with hydro-physico-chemical effects," *Chinese Journal of Rock Mechanics and Engineering*, vol. 27, no. 12, pp. 2540–2550, 2008.

[82] M. Wang, W. Wan, and Y. Zhao, "Determination of joint roughness coefficient of 2D rock joint profile based on fractal dimension by using of the gene expression programming," *Geotechnical and Geological Engineering*, vol. 38, no. 1, pp. 861–871, 2020.

[83] W. Yang, Q. Zhang, S. Li, and S. Wang, "Time-dependent behavior of diabase and a nonlinear creep model," *Rock Mechanics and Rock Engineering*, vol. 47, no. 4, pp. 1211–1224, 2014.

[84] Z. Chang, H. Gao, F. Huang, J. Chen, J. Huang, and Z. Guo, "Study on the creep behaviours and the improved burgers model of a loess landslide considering matric suction," *Natural Hazards*, vol. 103, no. 1, pp. 1479–1497, 2020.

[85] H. Lin, X. Zhang, Y. Wang et al., "Improved nonlinear nishihara shear creep model with variable parameters for rock-like materials," *Advances in Civil Engineering*, vol. 2020, Article ID 7302141, 15 pages, 2020.

[86] C. Zhang, Y. Wang, and T. Jiang, "The propagation mechanism of an oblique straight crack in a rock sample and the effect of osmotic pressure under in-plane biaxial compression," *Arabian Journal of Geosciences*, vol. 13, no. 15, p. 736, 2020.

[87] W. Xu, S. Yang, S. Xie, J. Shao, and Y. Wang, "Investigation on triaxial rheological mechanical properties of greenschist specimen (II): model analysis," *Yantu Lixue/Rock and Soil Mechanics*, vol. 26, pp. 693–698, 2005.